Effects of a Bearing Strut on the Performance of a Turbopump Inducer

Chang-Ho Choi,* Jun-Gu Noh,† Jin-Sun Kim,† Soon-Sam Hong,* and Jinhan Kim‡
Korea Aerospace Research Institute, Daejeon 305-333, Republic of Korea

DOI: 10.2514/1.19753

Experimental and computational studies on an inducer with and without a bearing strut were performed to evaluate the effects of a strut on the performance of an inducer. Global performance data, such as head rise and efficiency, and detailed flow characteristics, such as surface static pressures, were measured and compared with computational results. Generally, a good agreement is observed between experimental and computational results, but some discrepancies are observed due to complex flow features such as backflows at the inlet and strut/inducer interactions. For the flow rates where the backflow region is large, installing a strut enhanced the hydraulic performance of the inducer by diminishing the size of the backflows. The results also show that the strut has negligible effect on the suction performance of the inducer.

Nomenclature

A	=	inducer inlet area
C_p	=	static pressure coefficient, $=2(p - p_{1t})/(\rho U_{1t}^2)$
L	=	inducer axial length at hub
Q	=	volume flow rate
r^*	=	dimensionless radius, $=(r - r_h)/(r_s - r_h)$
U	=	speed of the blade
z	=	axial coordinate
β	=	blade or relative flow angle
η	=	efficiency
σ	=	cavitation number, $=2(p_{1t} - p_v)/(\rho U_{1t}^2)$
ϕ	=	flow coefficient, $=Q/(A_1 U_{1t})$
ψ	=	head coefficient, $=2(p_2 - p_{1t})/(\rho U_{1t}^2)$

Subscripts

b	=	blade
d	=	design
h	=	hub
s	=	shroud
t	=	tip or total
z	=	axial direction
1	=	inducer inlet
2	=	inducer outlet

I. Introduction

MODERN liquid-rocket-propulsion systems generally employ two types of propellant-feed cycles: pressure-feed and turbopump-feed cycles. Because high efficiency and thrust in the propulsion cycle entails high chamber pressure, a pressure-feed cycle is less desirable for highly loaded propulsion systems due to its excessively high tank pressure requirement. On the other hand, a turbopump-feed cycle leads to a comparatively lower system weight and improved performance [1,2]. Therefore, turbopump systems, which pressurize liquid oxidizers and fuels, are frequently employed to achieve a high specific impulse.

A typical turbopump system consists of an inducer, impeller, and volute, including seals, as shown in Fig. 1. An inducer is employed in a modern rocket feed system because it allows a turbopump system to operate at a high speed with low inlet pressures so as to minimize the weight and the size of the system. Cavitation performance can be improved by installing an inducer to the pump, thus increasing the operational speed of the pump. The main purpose of an inducer is to increase the static pressure before an impeller to enable the impeller to operate satisfactorily under cavitation environments. With the aid of the anticavitation function of the inducer, a centrifugal impeller can pump low-pressure propellants to high discharge pressures without cavitation breakdown [3,4].

Most turbopumps place bearings downstream of the inducer to achieve high-suction performance by removing obstacles upstream of the inducer as shown in Fig. 2. Therefore, most studies have been focused on the inducer flow phenomena without any obstacles upstream of the inducer [3–8]. However, a pump configuration with a bearing located upstream of an inducer is simple in design and is robust in reducing severe cavitation-induced shaft vibrations at the inlet. This study adopts a configuration with a bearing and strut located upstream of an inducer. The effects of a bearing strut on the performance of an inducer are investigated by both experimental and computational methods.

II. Inducer Design and Experimental Setup

Table 1 summarizes the design characteristics of the inducer under consideration. The inducer has a high solidity and moderate blade tip angle at the inlet. The experiments are conducted at a speed of 6000 rpm.

The experiments were performed at a test facility at the Korea Aerospace Research Institute, specially developed for hydraulic and suction performance tests of inducers [9]. An outline of the closed-loop test facility is shown in Fig. 3. The test inducer is driven by a variable-speed motor with a capacity of 10,000 rpm and 37 kW, and a torque meter is installed between the inducer and the motor. The flow rate is measured by a turbine flowmeter and controlled by an automatic regulating valve. The inducer is followed by an axisymmetric diffuser installed to provide a circumferentially uniform flow at the inducer exit.

Figure 4 shows a close-up view of the test section with and without the strut. Pressure taps on the shroud wall are also shown. The strut is located upstream of the inducer to support the rotating axis. The present inducer has a tapered tip with a radius decreasing along the axis in the direction of the flow. By designing this kind of a tapered

Presented as Paper 4452 at the 41st AIAA/ASME/SAE/ASEE Joint Propulsion Conference & Exhibit, Tucson Arizona, 10–13 July 2005; received 30 August 2005; revision received 27 July 2006; accepted for publication 1 September 2006.

*Senior Researcher, Turbopump Department, 45 Eoeun-Dong, Yuseong. AIAA member.
†Research Engineer, Turbopump Department, 45 Eoeun-Dong, Yuseong.
‡Head of Department, Turbopump Department, 45 Eoeun-Dong, Yuseong.

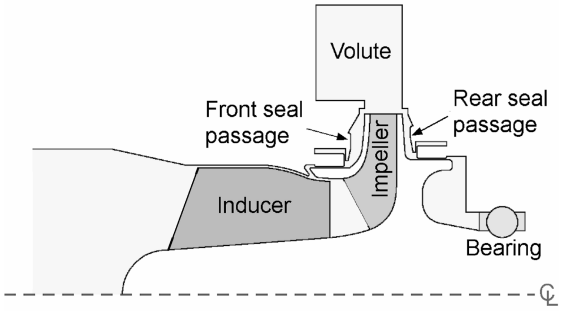

Fig. 1 Typical layout of a turbopump.

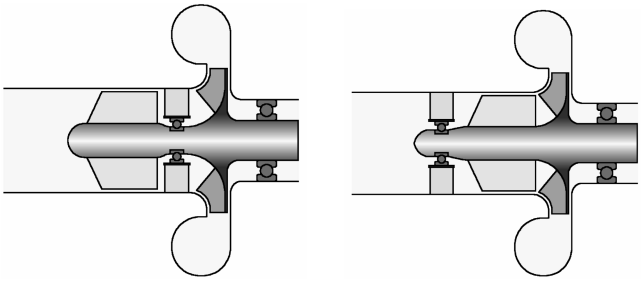

Fig. 2 Pump layout without and with the bearing upstream of an inducer.

shroud, the main impeller (Fig. 1) can have a high outlet-to-inlet diameter ratio and therefore obtain high hydraulic efficiency. The leading edge of the inducer is swept back to ensure blade structural robustness.

III. Computational Scheme

A commercial three-dimensional Reynolds averaged Navier–Stokes method is used in this study [10]. The method uses an explicit Runge–Kutta scheme and second-order accurate central-difference scheme with artificial dissipation for integration in time and space.

The k–ε turbulence model with an extended wall function is used to simulate turbulence effects. To accelerate the convergence to a solution, locally varying time steps, implicit residual smoothing, and multigrid schemes are applied to the governing equations.

A uniform flow condition is imposed at the inlet. Static pressures are assigned at the outlet of the inducer. Periodic boundary conditions are set at corresponding positions because only one blade passage is solved for the strut and the inducer. To simulate strut/inducer interaction, a mixing plane [11] is adopted that allows exchanges of only averaged flow properties. The mixing-plane method is useful in predicting overall flowfields with limited computational resources, but the method is inevitably disadvantaged in predicting detailed flowfields across the mixing plane, especially when flow separation occurs.

Figure 5 shows the geometry and the computational grid of the inducer with the strut, and Fig. 6 shows the location of the mixing plane for the computation. The value of y^+, the dimensionless quantity of the distance of the first grid point from the wall, is kept between 10 and 50 because the wall function is used. The diffuser installed downstream of the inducer is included for the calculation because it affected the inducer flow at partial flow rates. The grid sensitivity test was conducted with the half (coarse) and doubled (fine) size of the present grid (medium) for the case with the strut. Although the computations with the fine grid showed slightly better agreements with the experimental results than those with the others, the flowfield trends were almost the same regardless of the grid size. It was judged that the medium grid was fine enough to investigate the flow structure around the inducer. Therefore, the present grid was selected for the computations. The grid for the inducer only calculations was selected based on the previous study [12].

Table 1 Design characteristics of the inducer

Item		Value
Design flow coefficient (ϕ)		0.096
Blade number		3
Solidity at tip		2.7
Blade tip angle	Inlet (β_{1bt})	9.6 deg
	Outlet (β_{2bt})	15.0 deg
Radial tip clearance		1 mm
Angle variation on line normal to hub		$\tan(\beta_b) = (r_t/r)\tan(\beta_{bt})$

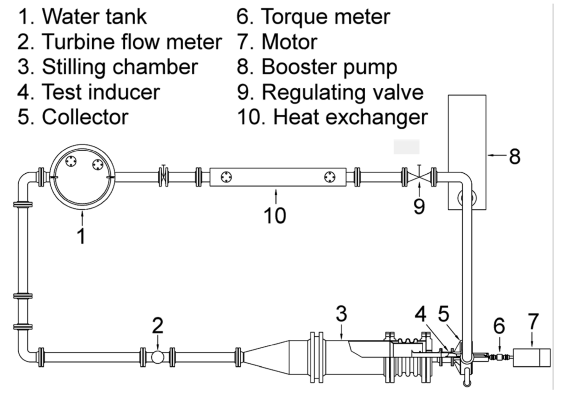

Fig. 3 Plane view of the inducer test rig.

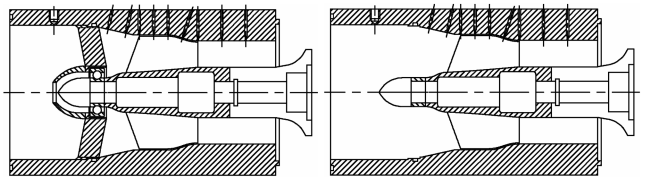

Fig. 4 Inducer test section with and without a bearing strut.

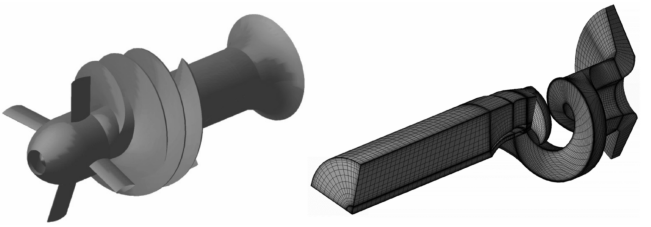

Fig. 5 Inducer geometry and computational grids (351,249 cells).

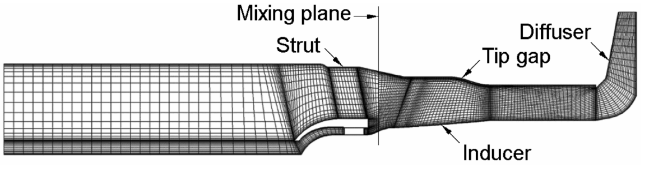

Fig. 6 Meridional grid for computations with the strut.

IV. Results and Discussions

Computations are performed at three flow rates: $1.0Q_d$ (design flow rate), $0.7Q_d$ (reduced flow rate), and $1.3Q_d$ (increased flow rate). Computations with and without the strut were performed.

Figure 7 shows circumferentially averaged streamline distributions along the meridional plane. Backflows occur at the inlet of the

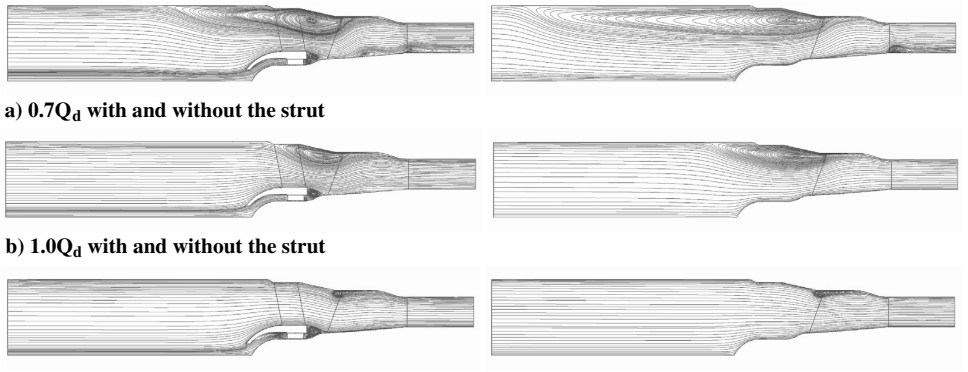

a) $0.7Q_d$ with and without the strut

b) $1.0Q_d$ with and without the strut

c) $1.3Q_d$ with and without the strut

Fig. 7 Circumferentially averaged streamline distributions at three operating points.

shroud and become stronger as the flow rate is reduced. It seems that the backflow is limited by the inlet boundary condition for the $0.7Q_d$ calculation without a strut. Calculations with the longer inlets were conducted, but the backflow was persistently observed stretching up to the inlet boundary for the $0.7Q_d$ calculation. These phenomena were also observed in the experiments. Therefore, the location of the inlet boundary was selected to save the computational time and to have the compact view by reducing the computational domain. Backflows are due to both the tip clearance and the large incidence angle that causes a rapid pressure rise at the inlet tip region for the reduced flows. Flow separation at the outlet is also observed at $0.7Q_d$. The separation caused by the diffuser extends to the inducer outlet when the flow rate is reduced, which justifies the additional computational cost of including the diffuser in the calculation [8]. The size of the backflow is reduced when the strut is installed. The strut hinders the backflows from extending far upstream. Figure 8 shows three-dimensional streamlines starting from the inducer inlet, which demonstrate the effect of a strut on the backflows. The fluid in the backflow rotates with the axis and flows upstream when the strut is not installed. On the other hand, when the strut is installed, the strut hinders the fluid from rotating about the axis and thus from extending upstream as shown in Fig. 8. Bario et al. [7] noted that the backflows can induce in-block rotation of the fluid in the tank, altering the global behavior of the pump when the backflows extend up to the tank. Therefore, the strut has favorable effects in preventing in-block rotation of the fluid in the tank by diminishing the size of the backflows.

Calculated static pressure distributions along the inducer shroud surface are presented in Fig. 9 in comparison with the experimental data. The computational data without the strut agree well with the experimental data for various flow rates. However, computational results with the strut differ from experimental ones due to strong strut/inducer interactions when the backflows reach the strut. As mentioned earlier, the mixing-plane method fails to predict the flowfield properly when the backflows move across the mixing plane. For inducer only computations, computational results near the

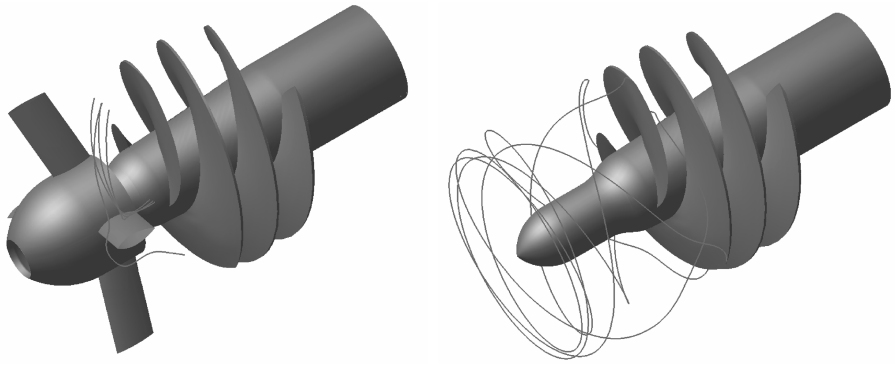

Fig. 8 Streamlines with and without the strut at $0.7Q_d$.

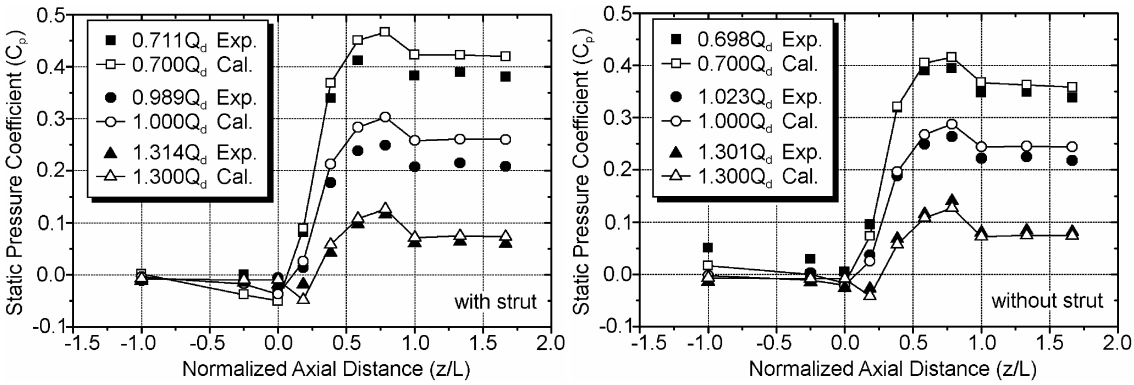

Fig. 9 Static pressure distributions along the shroud surface.

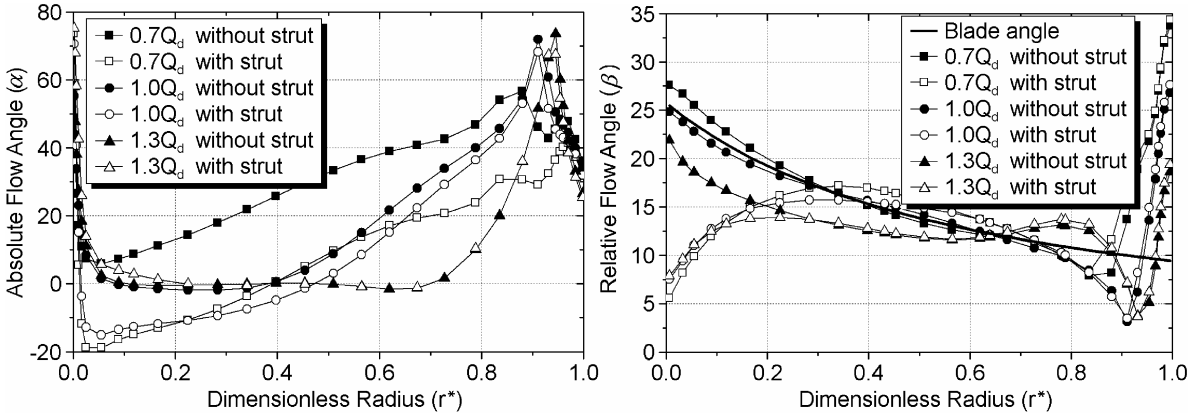

Fig. 10 Absolute and relative flow angle distributions near the inducer leading edge.

inlet ($z/L < 0.0$) differ from experimental ones due to the strong backflows at low flow rates. As the bubble size becomes bigger, it is disturbed by the inlet boundary where the uniform flow condition is imposed (see Fig. 7a). Thus, the predictions and the experiments agree well at the inlet for the high flow rate because the backflow size is small. The adverse pressure gradient increases near the inlet as the flow rate is reduced, which in turn increases the size of backflows. It is also seen that the static pressure decreases after $z/L = 0.5$ because the adopted inducer has a tapered shroud as shown in Fig. 4.

Figure 10 shows predicted flow angle distributions at the inducer leading edge. (Flow angles were not measured.) The absolute angles are almost uniform at $1.3Q_d$ regardless of the strut. However, the absolute angles increase from hub to shroud at the low flow rates. A prewhirl develops at the inlet due to the rotation of the inducer blades. The sweepback of the leading edge induces this kind of prewhirl [13]. The strength of the prewhirl (or absolute angle) decreases when a strut is present indicating that the strut acts like a guide vane. The strut prevents the flow from prerotation. The incidence angle becomes negative due to the strong backflows at low flow rates. For calculations with a strut, the incidence angle is positive near the hub ($r^* < 0.3$).

Inducer performance is presented in Fig. 11. The computation shows a similar trend to the experiment, although there are some discrepancies. Without a strut, the head decreases at reduced flows because the strong backflows cause increasing viscous losses. The inducer with a strut shows better performances than that without a strut at reduced flow rates, but the inducer with a strut shows worse performance than that without a strut at increased flow rates due to increased skin friction losses at the strut.

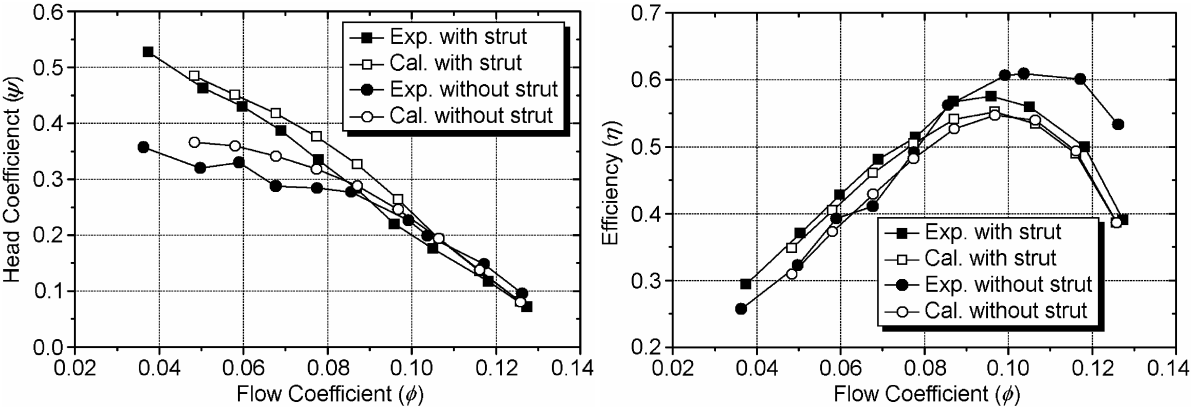

Fig. 11 Static head coefficient and efficiency distributions.

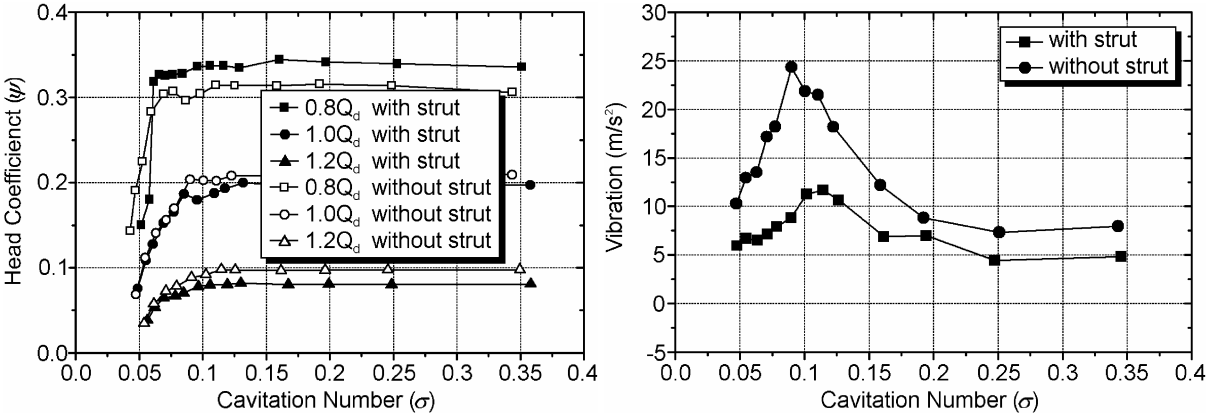

Fig. 12 Suction performance and vibration distributions.

Figure 12 shows the suction performance and the vibration measured on the surface of the bearing carrier installed between the inducer and torque meter. The vibration is measured only at the design flow rate. Suction performance calculations were not conducted due to the limitation of the CFD code. The suction performance of the inducer shows almost no difference between both measurements, although the head rises are slightly different. With a strut, the vibration reduces due to the function of the strut supporting the front axis of the inducer. The highest vibration occurs at the onset of the cavitation breakdown ($\sigma \approx 0.1$). The highest vibration level with the strut decreases up to 48% of that without a strut.

V. Conclusion

The effects of installing a strut on the performance characteristics of an inducer for applications in turbopumps were studied. The overall performance and the pressure on the shroud were measured and compared with the computational results. Numerical predictions generally agreed with experimental results, but some disagreements were observed, which may be attributed to the complexity of the strut/inducer interaction and backflows. The effects of installing a strut upstream of an inducer are as follows.

1) The size of the backflow decreases when the strut is installed ahead of the inducer as the strut prevents backflows from rotating about the axis, especially at reduced flow rates. Consequently, a drop in the developed head at the reduced flow was not observed for the inducer with a strut.

2) The suction performance of an inducer with a strut is almost the same as that without a strut.

References

[1] Huzel, D. K., and Huang, D. H., *Modern Engineering for Design of Liquid-Propellant Rocket Engines*, AIAA, Washington, D.C., 1992, Chap. 6.

[2] Manski, D., Goertz, C., Saβnick, H. D., Hulka, J. R., Goracke, B. D., and Levack, D. J. H., "Cycles for Earth-to-Orbit Propulsion," *Journal of Propulsion and Power*, Vol. 14, No. 5, 1998, pp. 588–604.

[3] Lakshminarayana, B., "Fluid Dynamics of Inducers-A Review," *Journal of Fluids Engineering*, Vol. 104, No. 4, 1982, pp. 411–427.

[4] Brennen, C. E., *Hydrodynamics of Pumps*, Oxford Univ. Press, Oxford, England, U.K., 1994.

[5] Kamijo, K., Yoshida, M., and Tsujimoto, Y., "Hydraulic and Mechanical Performance of LE-7 LOX Pump Inducer," *Journal of Propulsion and Power*, Vol. 9, No. 6, 1993, pp. 819–826.

[6] Lakshminarayana, B., *Analytical and Experimental Study of Flow Phenomenon in Noncavitating Rocket Pump Inducers*, NASA CR 3471, 1981.

[7] Bario, F., Faure, T. M., Jondeau, E., Normand, J. L., and Duc, J. M. N., "Analysis of Inducer Recirculating Inlet Flow," *Journal of Propulsion and Power*, Vol. 19, No. 4, 2003, pp. 521–528.

[8] Choi, C. H., Hong, S. S., Cha, B. J., and Yang, S. S., "Study on the Hydraulic Performance of a Turbopump Inducer," *Proceedings of the 2003 Joint ASME-JSME Fluids Engineering Summer Conference*, American Society of Mechanical Engineers Paper FEDSM2003-45095, 2003.

[9] Hong, S. S., Kim, J. S., Choi, C. H., and Kim, J., "Effect of Tip Clearance on the Cavitation Performance of a Turbopump Inducer," *Journal of Propulsion and Power*, Vol. 22, No. 1, 2006, pp. 174–179.

[10] *Fine/Turbo Manual*, Ver. 6.2-3, Numeca, Inc., Brussels, 2004.

[11] Choi, C. H., and Yoo, J. Y., "Unsteady Blade-Row Flows Calculations Using a Low-Reynolds Number Turbulence Model," *Journal of Propulsion and Power*, Vol. 16, No. 5, 2000, pp. 768–776.

[12] Choi. C. H., Hong, S. S., and Kim, J., "Numerical Study on the Hydraulic Performance Prediction of a Turbopump Inducer," *Journal of the Korean Society for Aeronautical and Space Sciences*, Vol. 31, No. 6, 2003, pp. 72–78 (in Korean).

[13] Choi. C. H., and Kim, J., "Numerical Study on the Hydrodynamic Performance of a Turbopump Inducer," *Proceedings of the 2004 Korean Society for Aeronautical and Space Sciences Fall Conference*, Korean Society for Aeronautical and Space Sciences, Seoul, Republic of Korea, 2004, pp. 958–963 (in Korean).

T. Wang
Associate Editor